JEM

Supplemental material

Xing et al., **https://doi.org/10.1084/jem.20171514**

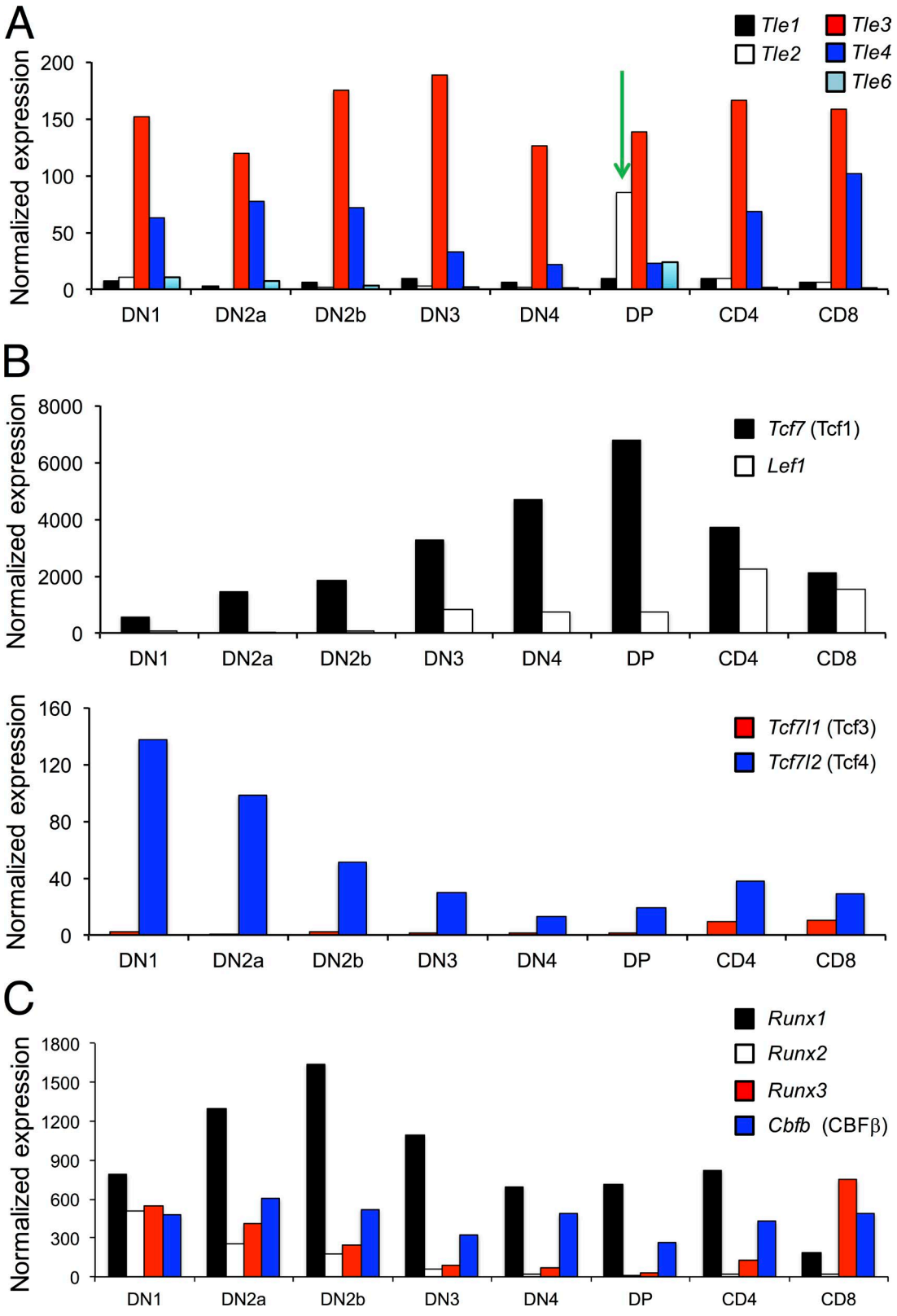

Figure S1. **Expression changes in Tle, Tcf/Lef, and Runx/CBF factors during T cell development. (A–C)** RNA-Seq data on thymocytes at various developmental stages were retrieved from the Immunological Genome Project. Duplicate samples were measured and the reads were processed and normalized with DESeq2. The average of normalized in expression was shown for *Tle* (A), *Tcf/Lef* (B), and *Runx* (C) genes. Note that *Tle2* shows strong up-regulation in DP thymocytes (green arrow in A) but is down-regulated in CD4 or CD8 single positive cells. *Tle5*, which encodes a truncated form of Tle protein, is not annotated as an independent gene, and its data are missing. In B, Tcf1 and Lef1 are highly expressed and displayed separately with a different y-axis scale. Gene symbols are in italic, and protein names, if different from gene symbols, are in parentheses.

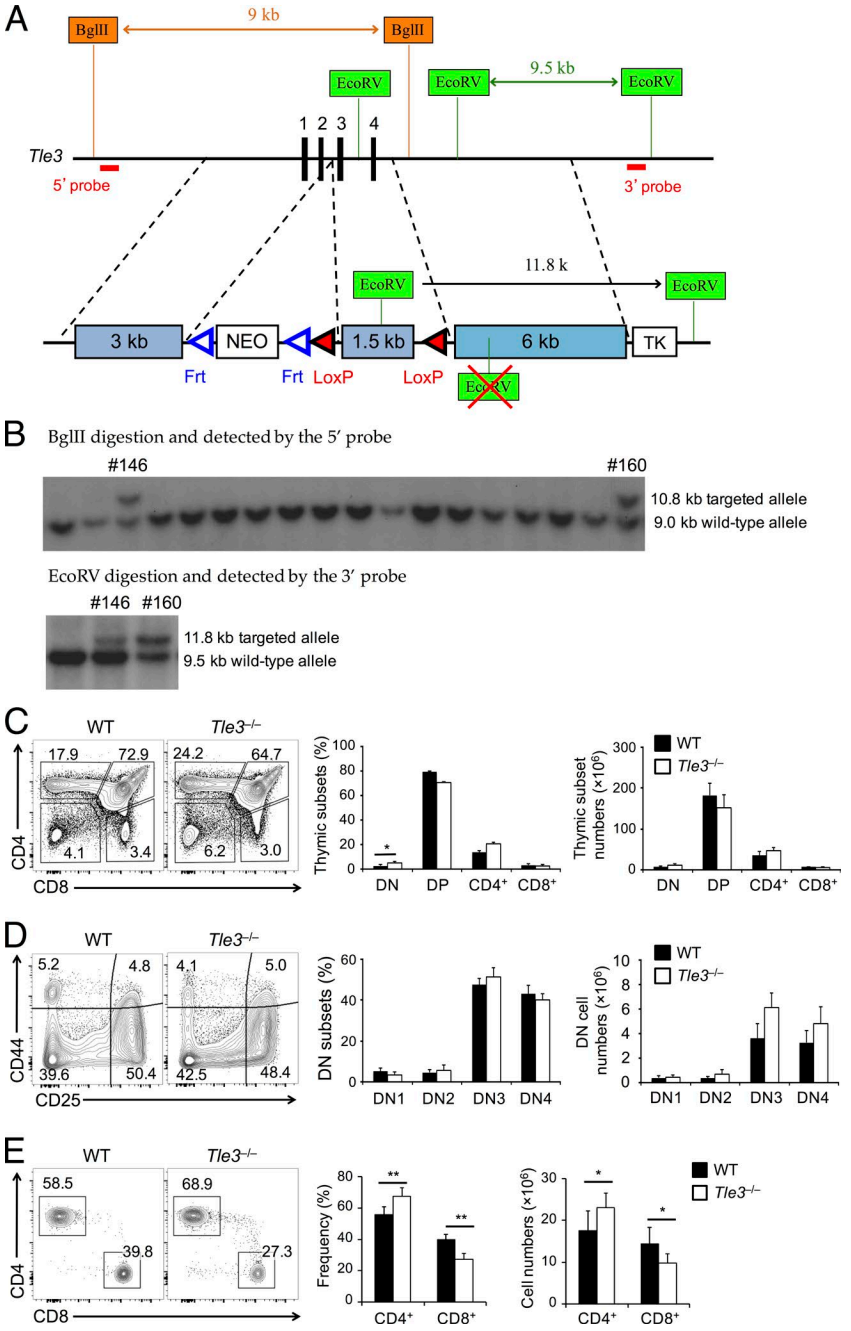

Figure S2. **Generation and characterization of *Tle3* conditionally targeted mice. (A)** Targeting strategy. Depicted on top are partial structure of the *Tle3* gene with vertical lines denoting exons (all numbered), key enzyme sites, and relative locations of 5′- and 3′-probes used in Southern blotting. Shown at the bottom is the structure of the targeting vector, highlighting the targeting arms (3-kb upstream arm and 6-kb downstream arm), locations of inserted LoxP sites (filled triangles in red), Frt sites (open triangles in blue), and neomycin resistant gene (NEO) cassette. Note that the EcoRV site within the 6-kb downstream targeting arm was destroyed to facilitate detection of a targeted allele by Southern blotting. **B**. Identification of ES cell clones with expected homologous recombination. Genomic DNA was extracted from ES cell clones generated after targeting construct electroporation and selection, digested with BglII, and blotted with the 5′-probe, which detects the WT allele at ~9 kb, and the targeted allele at ~10.8 kb (top panel). The positive clones (146 and 160) are marked. The genomic DNA from positive clones was then digested with EcoRV and blotted with the 3′-probe, which detects the WT allele at 9.5 kb, and the targeted allele at 11.8 kb. Clone 160 was used for blastocyst microinjection and generation of the $Tle3^{FL/+}$ mice. **(C)** Analysis of thymocyte maturation stages. Lineage-negative thymocytes from WT and $Tle3^{-/-}$ mice were stained for CD4 and CD8. The frequency of DN, DP, $CD4^+$ and $CD8^+$ thymocytes are shown in representative contour plot (left panels), and cumulative data on frequency and number of each subset are in middle and right panels, respectively. Data are means ± SD ($n \geq 4$ from at least two experiments). **(D)** Analysis of DN thymocytes. Lineage-negative $CD4^-CD8^-$ thymocytes from WT and $Tle3^{-/-}$ mice were stained for CD25 and CD44. The frequency of DN1–4 subsets are shown in representative contour plot (left panels), and cumulative data on frequency and number of each subset are in middle and right panels, respectively. Data are means ± SD ($n \geq 4$ from at least two experiments). **(E)** Analysis of peripheral T cells. $TCR\beta^+$ splenocytes from WT and $Tle3^{-/-}$ mice were stained for CD4 and CD8. The frequency of $CD4^+$ and $CD8^+$ T cells are shown in representative contour plot (left panels), and cumulative data on frequency and number of each subset are in middle and right panels, respectively. Data are means ± SD ($n \geq 6$ from at least two experiments). *, $P < 0.05$; ** $P < 0.01$ by Student's *t* test.

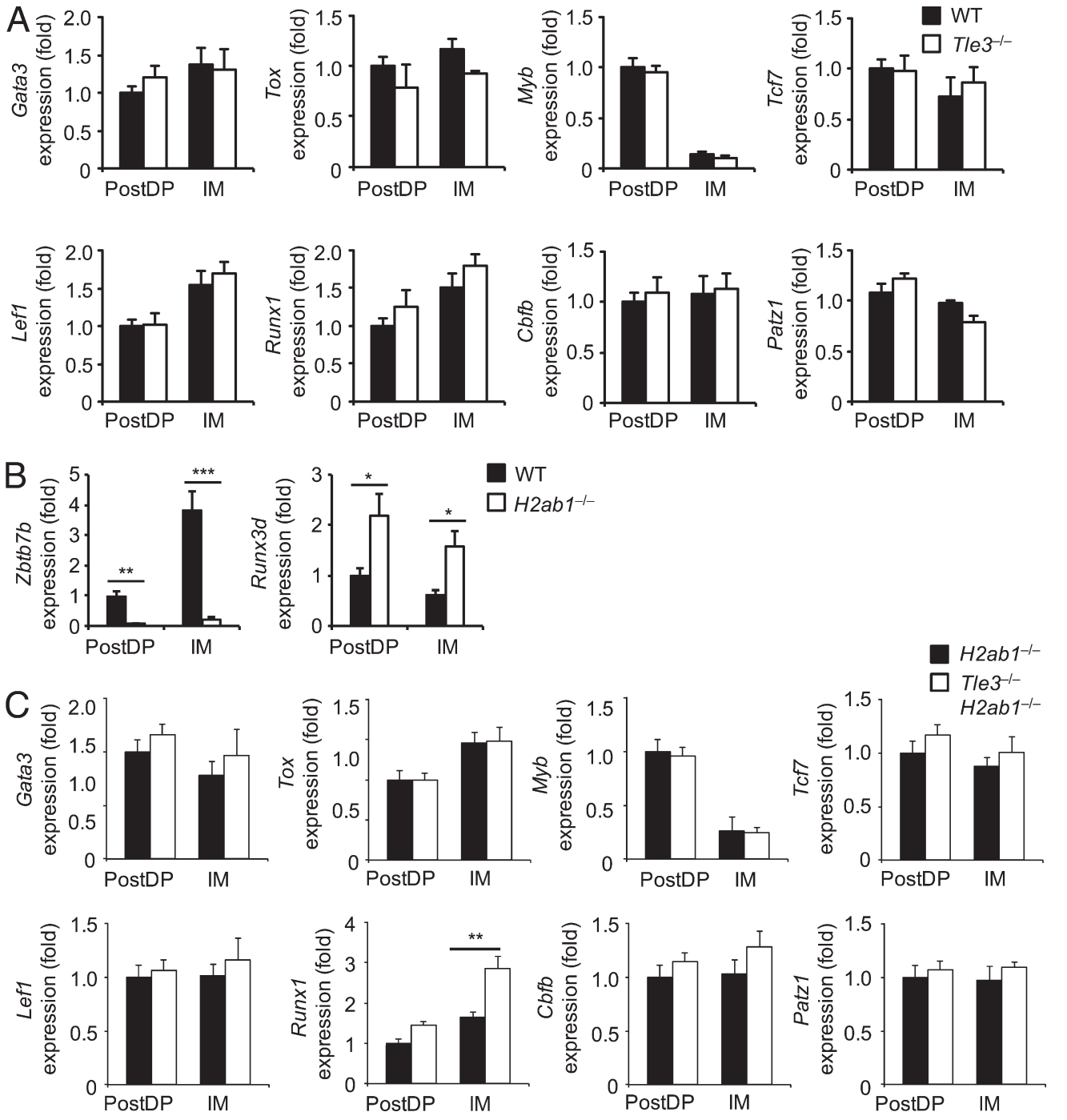

Figure S3. **Tle3 deficiency does not strongly affect the expression of lineage-specifying transcriptional regulators other than the ThPOK-Runx3 axis. (A)** Gene expression analysis in post-select DP and IM thymocytes sorted from WT or *Tle3*$^{-/-}$ mice. Total RNA was extracted from sorted cells, reverse-transcribed, and transcripts of indicated genes were determined by qPCR. For calculation of relative expression of each gene, its expression was first normalized to the *Hprt* house-keeping gene in the same cell type; the gene expression in WT PostDP cells were set at 1, and its relative expression in all other cell types were normalized accordingly. Data are means ± SD from two experiments (n = 4). **(B)** Gene expression analysis in post-select DP and IM thymocytes sorted from WT or *H2ab1*$^{-/-}$mice. Gene expression was determined as in A. Data are means ± SD from two experiments (n = 4). **(C)** Gene expression analysis in post-select DP and IM thymocytes sorted from *H2ab1*$^{-/-}$ or *Tle3*$^{-/-}$*H2ab1*$^{-/-}$ mice. Gene expression was determined as in A. Data are means ± SD from two experiments (n = 4). *, P < 0.05; ** P < 0.01; ***, P < 0.001 by Student's *t* test.

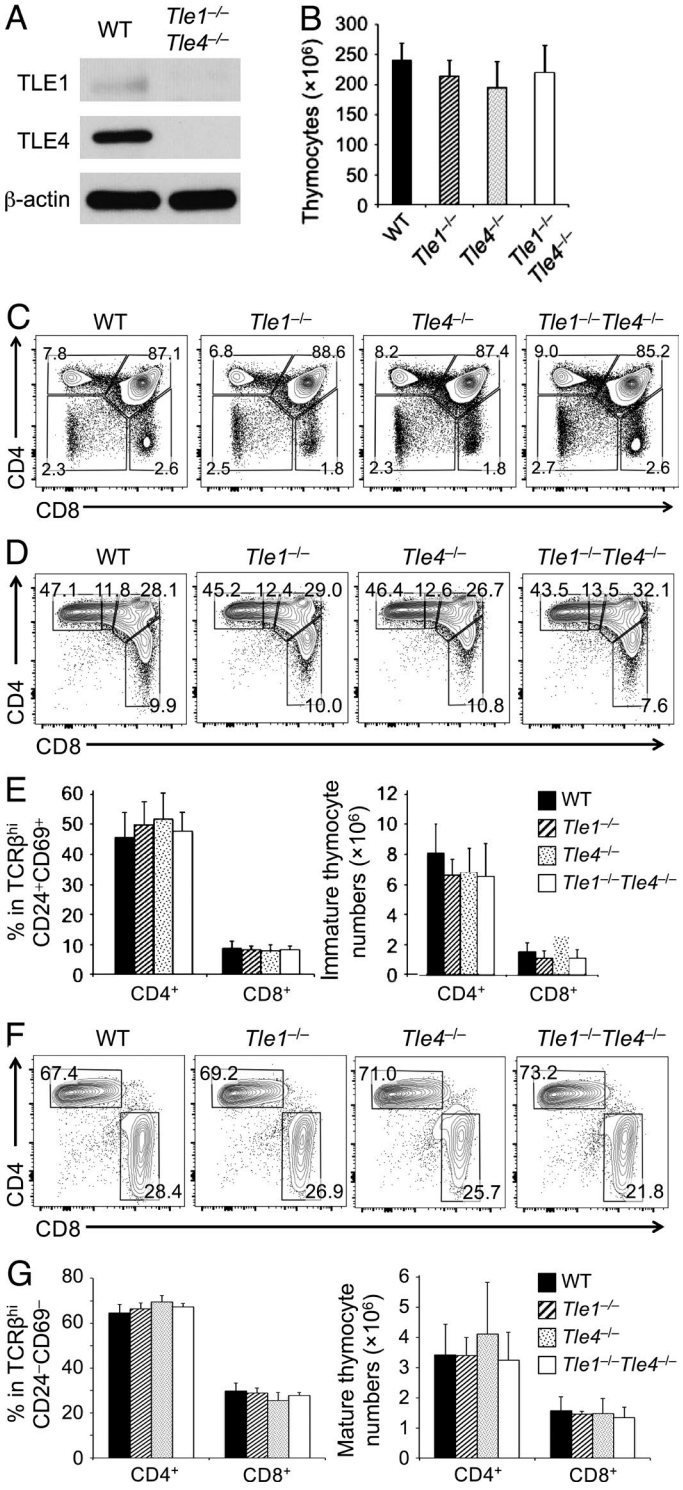

Figure S4. **Double deletion of Tle1 and Tle4 did not detectably perturb T cell development. (A)** Immunoblot of Tle1 and Tle4 proteins in total thymocytes from WT and *Tle1*$^{-/-}$*Tle4*$^{-/-}$ mice, with β-actin as loading control. Data are representative from two experiments. **(B)** Total thymic cellularity. Data are means ± SD (n = 9 for WT, 4 for *Tle1*$^{-/-}$, 3 for *Tle4*$^{-/-}$, and 6 for *Tle1*$^{-/-}$*Tle4*$^{-/-}$, analyzed in at least three experiments). **(C)** Characterization of thymocytes maturation stages in WT, *Tle1*$^{-/-}$, *Tle4*$^{-/-}$, and *Tle1*$^{-/-}$*Tle4*$^{-/-}$ mice. Lin^{-} thymocytes were stained for CD4 and CD8, and frequency of DN, DP, CD4^{+}, and CD8^{+} thymocytes are shown in representative contour plots. **(D and E)** Characterization of post-select immature thymocytes. TCRβ^{hi}CD69^{+}CD24^{+} post-select immature thymocytes from mice of indicated genotypes were detected for CD4^{+}, CD4^{+}CD8^{lo}, DP, and CD8^{+} populations (clockwise from top left in D). Cumulative data on frequency (left panels) and numbers (right panels) of CD4^{+} and CD8^{+} thymocytes are shown in E. Data are means ± SD. **(F and G)** Characterization of post-select mature thymocytes. TCRβ^{hi}CD69^{-}CD24^{-} post-select mature thymocytes from mice of indicated genotypes were detected for CD4^{+} and CD8^{+} populations (F). Cumulative data on frequency (left panels) and numbers (right panels) of CD4^{+} and CD8^{+} SP thymocytes are shown in F. Data are means ± SD. For C–G, n = 12 for WT, 6 for *Tle1*$^{-/-}$, 5 for *Tle4*$^{-/-}$, and 8 for *Tle1*$^{-/-}$*Tle4*$^{-/-}$ mice analyzed in at least three experiments. None of readouts among different genotypes showed statistically significant differences, as determined by one-way ANOVA coupled with *Bonferroni* correction for multiple group comparisons.

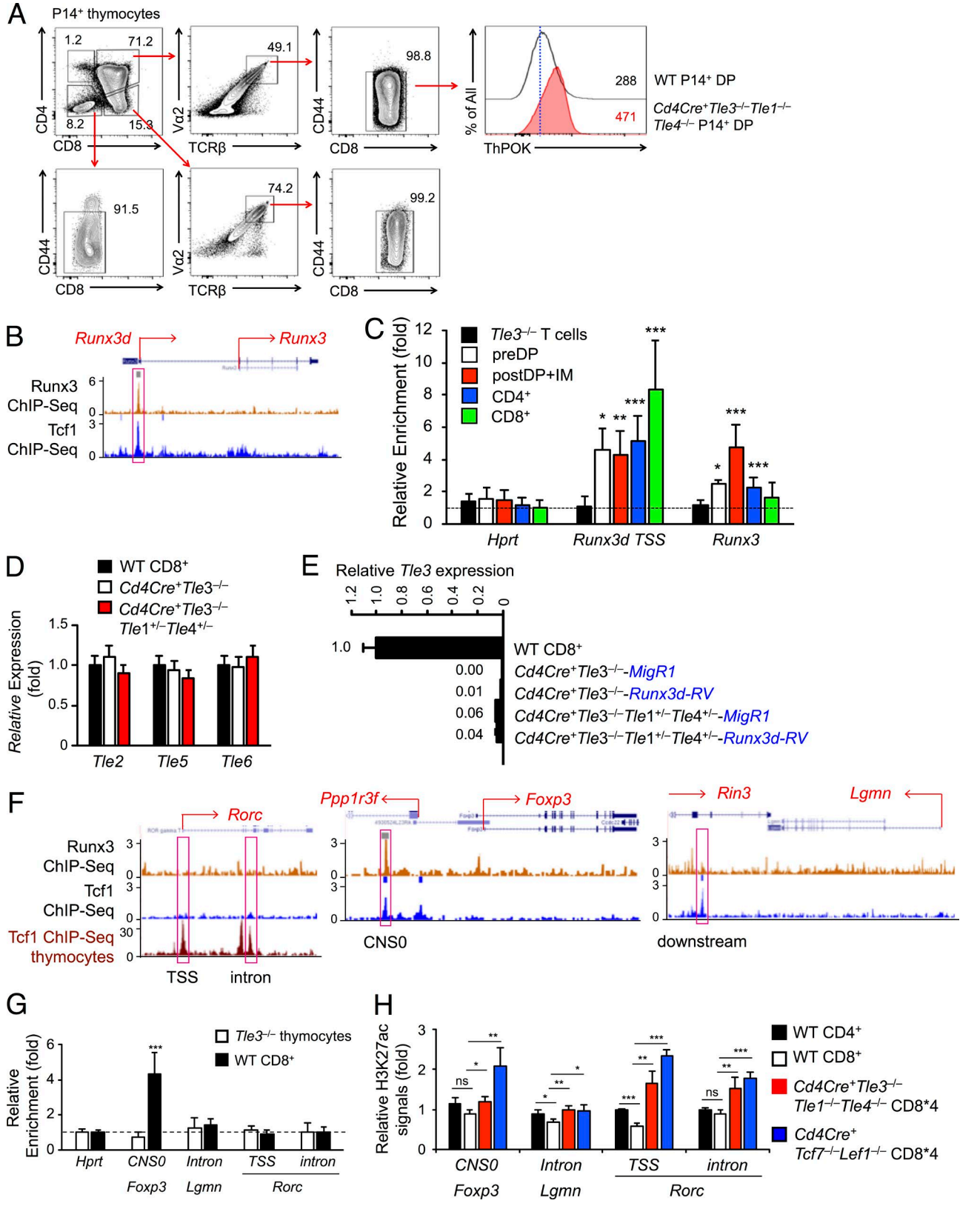
A
P14+ thymocytes
1.2
71.2
8.2
15.3
CD4
CD8
49.1
Vα2
TCRβ
98.8
CD44
CD8
288
471
% of All
ThPOK
WT P14+ DP
Cd4Cre+Tle3−/−Tle1−/−
Tle4−/− P14+ DP
91.5
74.2
99.2
B
Runx3d
Runx3
Runx3
ChIP-Seq
Tcf1
ChIP-Seq
C
Tle3−/− T cells
preDP
postDP+IM
CD4+
CD8+
Relative Enrichment (fold)
Hprt
Runx3d TSS
Runx3
D
WT CD8+
Cd4Cre+Tle3−/−
Cd4Cre+Tle3−/−
Tle1+/−Tle4+/−
Relative Expression (fold)
Tle2
Tle5
Tle6
E
Relative Tle3 expression
WT CD8+
Cd4Cre+Tle3−/−-MigR1
Cd4Cre+Tle3−/−-Runx3d-RV
Cd4Cre+Tle3−/−Tle1+/−Tle4+/−-MigR1
Cd4Cre+Tle3−/−Tle1+/−Tle4+/−-Runx3d-RV
F
Rorc
Ppp1r3f
Foxp3
Rin3
Lgmn
Runx3
ChIP-Seq
Tcf1
ChIP-Seq
Tcf1 ChIP-Seq
thymocytes
TSS
intron
CNS0
downstream
G
Tle3−/− thymocytes
WT CD8+
Relative Enrichment (fold)
Hprt
CNS0
Foxp3
Intron
Lgmn
TSS
intron
Rorc
H
Relative H3K27ac signals (fold)
WT CD4+
WT CD8+
Cd4Cre+Tle3−/−
Tle1−/−Tle4−/− CD8*4
Cd4Cre+
Tcf7−/−Lef1−/− CD8*4
CNS0
Foxp3
Intron
Lgmn
TSS
intron
Rorc

Figure S5. **Connection of Tle proteins with target genes. (A)** ThPOK expression is elevated MHC-I–restricted post-select DP thymocytes lacking Tle proteins. Shown in right panels is the flow cytometric analysis of thymocytes expressing the MHC-I–restricted P14 TCR transgene and gating strategy for $CD44^{lo\text{-}med}$ cells. The ThPOK expression was then detected by intracellular staining in $TCR\beta^+V\alpha2^+CD44^{lo\text{-}med}$ DP thymocytes from $P14^+$ WT or $P14^+$ *Cd4Cre*$^{+\text{-}}$ *Tle3*$^{-/-}$ *Tle1*$^{-/-}$ *Tle4*$^{-/-}$ mice. Values in the stacked histographs denote geometric MFI. Data are representative of two experiments (n = 3 for each genotype). **(B)** ChIP-Seq track at the *Runx3* gene locus in mature $CD8^+$ T cells. Tcf1 and Runx3 ChIP-Seq data were downloaded and displayed on the UCSC genome browser. Marked on top with red arrows is the transcriptional orientation from the distal and proximal TSSs of the *Runx3* gene. **(C)** ChIP analysis of enriched Tle3 binding at the *Runx3* gene locus. $TCR\beta^{lo\text{-}med}$ preselect DP thymocytes (PreDP), PostDP + IM thymocytes, and splenic $CD4^+$ and $CD8^+$ T cells were sort-purified from WT mice, and *Tle3*$^{-/-}$ cells were sorted as a negative control. The cells were used in ChIP with an anti-Tle3 antibody or control rabbit IgG. Relative enrichment of Tle3 binding was determined by normalizing anti-Tle3 to IgG signals at each indicated genomic location. Data are means ± SD from two to four experiments with each ChIP sample measured in duplicates. Dotted line marks no enrichment. *, P < 0.05; ** P < 0.01; ***, P < 0.001 by Student's *t* test compared with *Tle3*$^{-/-}$ cells. **(D)** Splenic $CD8^+$ T cells were sorted from mice of indicated genotype, RNA-extracted, and detected with quantitatively RT-PCR for *Tle1*, *Tle5*, and *Tle6* transcripts. The expression of each transcript in WT $CD8^+$ T cells was set as 1, and that in cells of other genotypes was normalized accordingly. Data are means ± SD from two experiments ($n \geq 4$). **(E)** Detection of *Tle3* transcripts in $CD8^+$ T cells derived from retrovirally infected BM cells. $CD45.2^+$ BM cells from *Cd4Cre*$^+$*Tle3*$^{-/-}$ or *Cd4Cre*$^+$*Tle3*$^{-/-}$*Tle1*$^{+/-}$*Tle4*$^{+/-}$ mice were infected with empty vector (*MigR1*) or *Runx3d*-expressing retrovirus (*Runx3d-RV*), followed by transplantation into irradiated $CD45.1^+$ recipients. 6 wk later, $CD45.2^+GFP^+CD8^+$ T cells were sort-purified from the recipient spleens, and the *Tle3* transcripts were detected by qRT-PCR. The primers were designed so that one was complementary to the floxed exon 3 and the other to exon 5 (outside of the floxed region). The *Tle3* expression in WT $CD8^+$ T cells was set as 1, and that in other cells was normalized accordingly. Data are means ± SD from two experiments ($n \geq 3$), and the values denote relative abundance of *Tle3* transcripts. **(F)** Tcf1 and Runx3 ChIP-Seq tracks at the *Foxp3*, *Lgmn*, and *Rorc* loci in $CD8^+$ T cells, with horizontal bars on top of each track denoting MACS-called binding peaks. **(G and H)** The neighboring genes and their transcriptional direction are also marked. Pink rectangles mark Tcf1 binding peaks that were assessed for Tle3 binding (G) and H3K27ac signals (H). For the *Foxp3* gene, the Tcf1 and Runx3 binding site is located upstream of *Foxp3* and in the intron region of *Ppp1r3f*, and this site overlaps with the CNS0 element (conserved noncoding sequence 0 for *Foxp3* gene) that is recently defined in Kitagawa et al. (2017) and Placek et al. (2017). For the *Lgmn* gene, the Tcf1 site is downstream of the gene body and in the intron region of *Rin3*, but not cooccupied by Runx3. For the *Rorc* gene, the third track in brown is Tcf1 ChIP-Seq track in total thymocytes (GSE46662, in Li et al., 2013), which are predominantly $CD4^+CD8^+$ double positive (DP) thymocytes. Tcf1 binding peaks were detected at the TSS and intron regions, likely derived from DP thymocytes, but neither Tcf1 nor Runx3 binding was found at this locus in mature $CD8^+$ T cells. **(G)** Enriched Tle3 binding is detected at *Foxp3* CNS0 but not *Lgmn* and *Rorc* loci. Tle3 ChIP was performed on WT splenic $CD8^+$ T cells with VavCre$^+$*Tle3*$^{FL/FL}$ (*Tle3*$^{-/-}$) total thymocytes as a negative control, and relative enrichment of Tle3 binding was determined at the indicated genomic locations. Data are means ± SD from 2 independent experiments with each ChIP sample measured in duplicates or triplicates. Dotted line marks no enrichment. ***, P < 0.001 by Student's *t* test. Note that *Foxp3* CNS0 is reported to promote Foxp3 expression in $CD4^+$ T cells, and is occupied by multiple transcriptional and epigenetic regulators including Satb1, Ets1, Bcl11b, Foxp3, Runx1, and MLL4 in regulatory T cells (Kitagawa et al., 2017; Placek et al., 2017). **(H)** H3K27ac status at the *Foxp3*, *Lgmn*, and *Rorc*. $CD8^*4$ cells were sorted from $TCR\beta^+$ splenocytes in *Cd4Cre*$^+$*Tle3*$^{-/-}$*Tle1*$^{-/-}$*Tle4*$^{-/-}$ and *Cd4Cre*$^+$*Tcf7*$^{-/-}$*Lef1*$^{-/-}$ mice, along with splenic $CD4^+$ and $CD8^+$ SP T cells from WT mice. The cells were subjected to H3K27ac ChIP analyses at indicated genomic locations. The H3K27ac signal was first normalized to chromatin input in each cell type, and that in WT $CD4^+$ T cells was set as 1, with relative H3K27ac in other cell types normalized accordingly. Data are means ± SD from two independent experiments with each ChIP sample measured in duplicates or triplicates. ns, not statistically significant; *, P < 0.05; **, P < 0.01; ***, P < 0.001 by Student's *t* test compared with WT $CD8^+$ T cells. Increased H3K27ac was more pronounced at *Foxp3* CNS0 in Tcf1/Lef1-deficient $CD8^*4$ cells, consistent with Tcf1 binding to this location and its intrinsic HDAC activity. Increased H3K27ac at *Rorc* TSS and intron region was also readily detectable in Tcf1/Lef1-deficient and Tle1/3/4-deficietn $CD8^*4$ cells, in spite of lacking direct binding by Tcf1 and Tle3 at this locus in $CD8^+$ T cells. We speculate that Tcf1 may have bound to *Rorc* in DP thymocytes but the binding is lost during differentiation to $CD8^+$ T cells; when Tcf1/Lef1 and/or Tle proteins are ablated by *Cd4Cre* in DP thymocytes, this locus becomes hyperacetylated, which was epigenetically inherited into $CD8^+$ T cells lacking either set of proteins.

https://doi.org/10.1084/jem.20171514

Table S1. **Primers for qRT-PCR**

Gene symbol	5′ primer	3′ primer
cDNA primers		
Hprt	5′-GCGTCGTGATTAGCGATGATG	5′-CTCGAGCAAGTCTTTCAGTCC
Runx3	5′-AGGGAAGAGTTTCACGCTCA	5′-AGGCCTTGGTCTGGTCTTCT
Runx3d	5′-CCAACCAAGTGGGTCTGAAC	5′-GTGCTCGGGTCTCGTATGAA
Zbtb7b	5′-CCCTGCTCGAGTTTGCTTAC	5′-CTCGCTCACAGTCATCCTCA
Gata3	5′-CTTATCAAGCCCAAGCGAAG	5′-CATTAGCGTTCCTCCTCCAG
Lef1	5′-TGAGTGCACGCTAAAGGAGA	5′-CTGACCAGCCTGGATAAAGC
Tcf7	5′-CCCCAGCTTTCTCCACTCTA	5′-CACAGTATGGGGGAGCTGTC
Cbfb	5′-GGAGATCGCTTTTGTGGCTA	5′-TCAGAATCATGGGAGCCTTC
Myb	5′-AACGACGAAGACCCTGAGAA	5′-GGGTAGCTGCAAGTGTGGTT
Runx1	5′-GGGATCCATCACCTCTTCCT	5′-GACGGCAGAGTAGGGAACTG
Patz1	5′-AAGGTTTCTCCAGGCCAGAT	5′-GGCCCGCAAGTACTTTCCAC
Tox	5′-GAGGATGCCTCCAAGATCAA	5′-GCCTGGGTATCACGAAAGAA
Tle1	5′-CCGTCTCTCAGCTGGATTGT	5′-CTGCAGCATGAGAAGCAGAC
Tle2	5′-AGACAGTCCAGCCTCCTTGG	5′-AGAGGTGACTGGCTGAGCTG
Tle3	5′-AACATTGCGGTTTGGGATCT	5′-TGCTGTAACTGCCGTCCTTC
Tle4	5′-CAACAACTCCAAGCTCAGCA	5′-TCATGGTGCTTCTTCTCATCC
Tle5	5′-GCGACTGACATGATGTTTCCG	5′-TCGGAGGTGGTGAACTTGAG
Tle6	5′-GGATATGGGACCTACGGACTC	5′-CAGTGACACCTTGGCCATC
Tle3-exon3-5	5′-TGACAAGCTGGCTAACGAGA	5′-GGCATGATCTGGGCTAGGAT
Nkg7	5′-TCCTCACTTCTCTGCCCACT	5′-GCAAGACAGAACCAGGAAGC
Itgae	5′-ATTTGGGGACCCTCTCAATC	5′-GGTCTGAGGCAATCAGCTTC
St8sia6	5′-GCTACGAGGTGGAAAGCAAG	5′-TGAGAATTCCCCCATTACCA
Itgb3	5′-TGTCGTCAGCCTTTACCAGA	5′-GGATTTTCCCGTAAGCATCA
Lgmn	5′-ACACCGGAGAGGATGTGACT	5′-CCGTGGTCGGTGAAGTAAAT
Cd40lg	5′-GGCAATTTGAAGACCTTGTCA	5′-CTGCATTACTGTTGGCTTCG
Foxp3	5′-AGAAGCTGGGAGCTATGCAG	5′-TACTGGTGGCTACGATGCAG
Rorγt	5′-GGACAGGGAGCCAAGTTCTCAG	5′-CACAGGTGATAACCCCGTAGTGG
Nrp1	5′-TGGTGGAATTGCTGTGGATG	5′-GGCTTCCTGGAGATGTTCTTG
Sytl2	5′-GAAGAGGAAGACAGCACCAG	5′-CTCAACAGTGGGAGGTCAAG
St3gal2	5′-CCTGGACCTAATGTGGATTGC	5′-GGTCCACCTGTCGTGAATG
Tmem64	5′-ACTTGGGAACCACACTACGG	5′-ACTTGAGCGCGATGGACTAC
Tbc1d4	5′-CCAGGAGGCACTTATAATGGAG	5′-TCCTGCAGCACGTGATATTC
Plxdn1	5′-TCAGCGAGCAGGAAATGAAC	5′-GCCATGATCTGTGGTCGATAC
Gata3	5′-CTTATCAAGCCCAAGCGAAG	5′-CATTAGCGTTCCTCCTCCAG
Genomic DNA primers		
Hprt	5′-GGTGAAGGTCGGAGTCAACG	5′-ATGAAGGGGTCATTGATGGC
Zbtb7b-GTE	5′-AGCCCTGGGTTCTTCTCTTC	5′-CCTCCTTTCTTTCCCCTTTG
Zbtb7b-silencer	5′-AACCCACCTGAAGAGGCGGTG	5′-TCCCAGCGGCGATTAGCACTG
Cd4-silencer	5′-GAACCACAAGGGTCGCTTAG	5′-CACAGTGACAGCCTGTGGTC
St8sia6-intron2	5′-AAACCTCTGCAAAGATGGGC	5′-ACAGGAAATGGGATGGTGGT
St8sia6-intron3	5′-ACCAGAGACCTAAGAGCTTCC	5′-TCCTTTCGTTTCTCTGCCTCT
Itgb3-intron	5′-GATCTCTGGGCCTTTGATCG	5′-CCCTGTATCCTTGCACCCTG
Itgb3-3′UTR	5′-CTTGCTTTGTCAGGCCATTC	5′-AGACTTGACACCACTTCCTCT

Gene symbol	5′ primer	3′ primer
cDNA primers		
Runx3d-TSS	5′-TTTTCCTTTCAGCCTCCAAA	5′-ATTGGCTAGGCCACTGTCAC
Runx3-TSS	5′-CCAACTTCCTCTGCTCCGT	5′-CCCTGCACTCACCTTGAAG
Foxp3-CNS0	5′-CTGATCTAGCAGCGCACAC	5′-GGTTCCCAACGTGACTTGAG
Lgmn-downstream	5′-GGAGAGGTAGGTCACAGCAT	5′-CCTACTCAGCTCAAGGACCA
Cd40lg-intron4	5′-CCTGCCTCCCACCTTTCA	5′-GGTTCAAAGTGGTGTGTGCA
Rorc-TSS	5′-GGAGCTGGTGGAGTCTGGTA	5′- GCAGTTGGAGGCACAAAGAT
Rorc-intron3	5′-AAGCGAAAGGAAACATGCAG	5′- GGTGGCTTGCTTCTGAACAT

References

Kitagawa, Y., N. Ohkura, Y. Kidani, A. Vandenbon, K. Hirota, R. Kawakami, K. Yasuda, D. Motooka, S. Nakamura, M. Kondo, et al. 2017. Guidance of regulatory T cell development by Satb1-dependent super-enhancer establishment. *Nat. Immunol.* 18:173–183. https://doi.org/10.1038/ni.3646

Li, L., J.A. Zhang, M. Dose, H.Y. Kueh, R. Mosadeghi, F. Gounari, and E.V. Rothenberg. 2013. A far downstream enhancer for murine Bcl11b controls its T-cell specific expression. *Blood.* 122:902–911. https://doi.org/10.1182/blood-2012-08-447839

Placek, K., G. Hu, K. Cui, D. Zhang, Y. Ding, J.E. Lee, Y. Jang, C. Wang, J.E. Konkel, J. Song, et al. 2017. MLL4 prepares the enhancer landscape for Foxp3 induction via chromatin looping. *Nat. Immunol.* 18:1035–1045.